### Title

Direct Embedment and Alignment of Silver Nanowires by Inkjet Printing for Stretchable Conductors




### Journal

ACS Applied Electronic Materials, 2(10)

### ISSN

2637-6113



### Authors

Al-Milaji, Karam Nashwan
Huang, Qijin
Li, Zhen
et al.



### Publication Date

2020-10-27

### DOI

10.1021/acsaelm.0c00616

Peer reviewed

ACS APPLIED ELECTRONIC MATERIALS

pubs.acs.org/acsaelm Article

# Direct Embedment and Alignment of Silver Nanowires by Inkjet Printing for Stretchable Conductors

Karam Nashwan Al-Milaji,[§] Qijin Huang,[§] Zhen Li, Tse Nga Ng, and Hong Zhao*

Cite This: *ACS Appl. Electron. Mater.* 2020, 2, 3289−3298 Read Online

ACCESS | Metrics & More | Article Recommendations | Supporting Information

**ABSTRACT:** Stretchable conductors have attracted tremendous attention owing to their potential applications as electrodes and sensing elements for wearable electronic devices. In this study, we have developed an inkjet printing process to directly embed and align silver nanowires in the polydimethylsiloxane elastomer for stretchable conductors. Instead of printing on top of elastomers, we printed the silver nanowires directly into an uncured liquid elastomer layer to embed the conductive nanowires, therefore eliminating the problems with surface wetting and delamination in conventional approaches, where the conductor is patterned on top of elastomers. This study investigated the process controls to tune the embedment depth and alignment of silver nanowires through inkjet printing. The printing process was captured with a high-speed camera to elucidate the mechanisms that direct the printed features. By controlling the thickness of the liquid elastomer layer and the post-printing treatment of printed lines, stretchable conductors composed of embedded silver nanowires have been fabricated in a single step. Because of the reflow of the viscous liquid elastomer, the printed silver nanowires are aligned along the printing direction, resulting in linewidth of tens of micrometers upon solvent removal. The stretchable conductors showed good mechanical and electrical stability under repeated bending and stretching/releasing cycles. This method of directly embedding silver nanowires into a liquid elastomer offers facile heterogeneous integration for digital patterning of stretchable electronics.

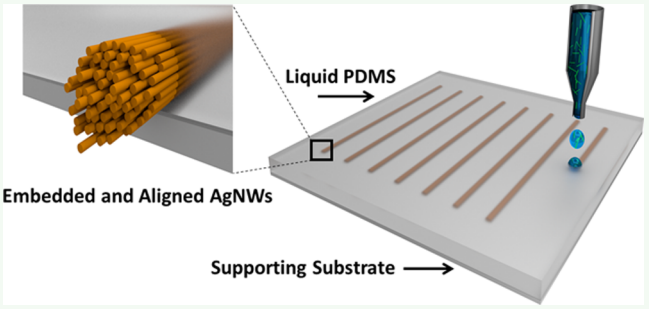


**KEYWORDS:** *inkjet printing, silver nanowires, alignment, stretchable conductors, flexible electronics*



## 1. INTRODUCTION

Stretchable electronics have drawn tremendous interest in the past few years,[1−5] as they provide new form factors for numerous applications, such as light-emitting diodes (LEDs),[6−8] thin-film transistor,[9,10] energy-harvesting and energy-storage devices,[11−13] and deformable conductors for human−machine interfaces.[14−17] Stretchable conductors are vital and indispensable components of soft electronics because of their significant roles in interconnectors and sensing devices.[18−21]

A variety of conductive nanomaterials, such as metal nanowires, carbon nanotubes, and graphene have been actively explored for stretchable conductors. Among these conductive materials, silver nanowires (AgNWs) are intensively investigated because of the excellent electrical conductivity and versatile fabrication processes.[22−24] Several strategies have been developed so far to integrate AgNWs into stretchable conductors. Conventional fabrication processes of stretchable conductors are achieved by depositing AgNWs on top of elastomer substrates or embedding AgNWs at the surface of elastomer substrates by transfer processing.[25−27] However, it is challenging to create a uniform deposition directly on top of elastomers, particularly the polydimethylsiloxane (PDMS), because of its hydrophobic nature. Plasma treatment of the elastomer substrate is often applied, but surface wettability is difficult to control on the treated hydrophilic surfaces as they undergo "hydrophobic recovery".[28] In addition, mechanical instability, represented by delamination, buckling, and fracturing of the deposited/transferred AgNWs after cyclic loading, leads to an irreversible increase in electrical resistance, which hinders the performance of the stretchable conductors. Recent studies have shown that the direct embedment of conductive materials into liquid elastomers provides an effective and facile approach to fabricate stretchable conductors, which can potentially overcome the aforementioned problems.[29,30]

For one-dimensional AgNWs, the electrical performance along the direction of alignment can be significantly improved by manipulating the nanowire orientation. This provides an effective way to enhance the performance of conductors, where the current only needs to flow in one direction.[31] Various

Received: July 18, 2020
Accepted: September 3, 2020
Published: September 3, 2020





https://dx.doi.org/10.1021/acsaelm.0c00616
*ACS Appl. Electron. Mater.* 2020, 2, 3289−3298

assembly strategies have been developed to align AgNWs, for example, microchannel alignment,[32] shear and flow alignment,[33−35] and capillary-assisted alignment.[36] However, these assembly strategies are more applicable in generating coatings and films, instead of patterning and on-demand printing processes. The alignment of AgNWs has been demonstrated in electrohydrodynamic printing because of its small features and narrow linewidth.[37,38] Nevertheless, the alignment of AgNWs has not been achieved in conventional inkjet printing.[25,39,40] Therefore, the embedment and alignment of AgNWs by an inkjet printing process could serve as an effective way to improve the performance of the printed stretchable conductors.

In this study, we have fabricated stretchable conductors by employing the inkjet printing technique, where colloidal droplets of AgNWs were directly printed and embedded into an uncured liquid PDMS layer. Compared with the conventional approaches where the conductor is patterned on top of elastomers, this method eliminates the problems with surface wetting and delamination on the elastomer surface. The single step of embedment and alignment of the AgNWs were achieved by controlling the thickness of the liquid PDMS layer and the post-printing treatment. Upon solvent evaporation, the viscous PDMS liquid shapes the printed AgNW lines into tens of micrometers in diameter, which significantly enhances the printing resolution as compared with that of the conventional inkjet printing process. Moreover, the printed AgNW lines exhibit alignment along the printing direction, which enhances the electrical performance of the fabricated stretchable conductors during multiple bending and stretching/releasing cycles. This study investigates the process controls to tune the embedment depth and alignment of AgNWs through inkjet printing.

## 2. EXPERIMENTAL SECTION

**2.1. Materials.** Polyethylene terephthalate (PET) films (MELINEX ST505) with 125 $\mu$m thickness were supplied by TEKRA, a division of EIS. Polyvinylpyrrolidone (PVP-K30) and silver nitrate (99%, ACS reagent) were purchased from Sigma-Aldrich. PDMS precursor and curing agent (Sylgard 184) were obtained from Dow Corning. KOPTEC ethanol (99.5% purity), acetone (99.5% purity), isopropanol (99.5% purity), and ethylene glycol (100% purity) were acquired from VWR. Deionized (DI) water with a resistivity of 18.2 MΩ·cm was produced by a Direct-Q water purification system (Millipore Sigma). All materials were used as received without further purification.

**2.2. Preparation of Liquid PDMS Layers.** The PDMS base was mixed with the curing agent in the proportion of 10:1 by weight to prepare the PDMS precursor. The precursor was put into a vacuum chamber to remove air bubbles. PET films were used as supporting substrates to deposit the liquid PDMS precursor. The films were rinsed by isopropanol and DI water, respectively, then dried with compressed air. After cleaning, the PET substrates were coated with liquid PDMS using the drop casting method to produce an elastomer layer with ∼1.5 mm thickness. Thinner PDMS layers were obtained by spin-coating at 600, 1000, and 3000 rpm for 20 s to produce layers with thicknesses of 250, 100, and 40 $\mu$m, respectively.

The viscosity of the freshly prepared PDMS was measured by a rheometer (Physica MCR-301, Anton Paar) using plate/plate geometry (50 mm in diameter) with a gap of 1 mm. Fixed measurement points were selected with a linear shear strain rate ramping from 0.01 to 100 $s^{-1}$. After measuring the viscosity of the fresh PDMS, the measurements were repeated after 30 min to mimic the experimental conditions.

**2.3. Preparation of AgNW Inks.** AgNWs with an average diameter of ∼100 nm and an average length of ∼14.5 $\mu$m (Figure S1) were chemically synthesized using a modified polyol reduction method.[41,42] Briefly, 0.5 g of polyvinylpyrrolidone (PVP) was added to 50 mL of ethylene glycol in a round-bottomed flask under a stirring speed of 400 rpm. The solution was kept at 170 °C in an oil bath for 1 h to form a homogeneous solution. Then, 150 $\mu$L of 0.1 mmol $L^{-1}$ NaCl/ethylene glycol solution was added into the homogeneous solution. After 10 min, 0.5 g of silver nitrate ($AgNO_3$), dissolved in 50 mL of ethylene glycol, was dripped into the flask with a volumetric flow rate of 2.5 mL $min^{-1}$. The reaction was continued for another 20 min at 170 °C. Finally, the flask was cooled down to room temperature, and the AgNWs were precipitated with acetone and centrifuged at 3000 rpm for 20 min. The AgNWs were washed three times with ethanol through centrifugation to remove the excess PVP, then re-dispersed in ethanol to obtain a solid concentration of 10 mg $mL^{-1}$ for the inkjet printing process. It is worth noting that by optimizing the printing parameters, the as-synthesized AgNWs were utilized (without ultrasonication) to fabricate the stretchable conductors.

**2.4. Fabrication of Embedded AgNW Lines.** Printing of AgNW ink was performed on an inkjet printing platform (Jetlab 4, MicroFab). The printing station was driven by a waveform generator (Jetdriver III, MicroFab) with an 80 $\mu$m nozzle (MJ-ATP-01-80-8MX, MicroFab). The printing frequency was set to 500 Hz to generate a stable jet with an inflight droplet size of ∼400 pL and droplet speed of 1.2 m/s. Different printing passes with 50 $\mu$m in-line droplet spacing and 25 $\mu$m shift among the printing passes were utilized to fabricate the embedded AgNW lines. The number of printing passes directly controls the amount of AgNWs in the printed lines.

In order to investigate the effect of drying conditions on the morphology of the printed lines, the printed samples were subjected to three different drying conditions (i.e., post-printing treatment): (i) curing the samples immediately after printing for 10 min at 90 °C, (ii) retaining the samples for 30 min at room temperature then curing for 10 min at 90 °C, and (iii) curing the samples at room temperature for 24 h. After ethanol evaporation and curing the PDMS layer, the stretchable conductors composed of embedded AgNW lines peeled off the PET substrate for electrical performance evaluation.

**2.5. In Situ Observation of the Droplet Embedment Process.** Droplet embedment into liquid PDMS was investigated in situ by the high-speed photography. AgNW colloidal droplets were directly jetted onto the liquid PDMS in a 25 mm × 25 mm × 10 mm glass container. A high-speed camera (Phantom, Miro LAB 3a10) at 1000 fps was used to monitor the droplet impact and embedment, along with a microscopic lens (Infinity Model K2 DistaMax) and an LED light source.

**2.6. Morphonology Characterization and AgNW Orientation Analysis.** The microstructures and alignment of the printed AgNWs assembly were characterized by field-emission scanning electron microscopy (SEM, HITACHI SU-70), operated at 5 kV. In order to clearly observe the AgNWs under the SEM, the uncross-linked PDMS was dissolved by cyclohexane after printing and retaining the sample for 30 min, leaving the AgNWs on the substrate for SEM characterization. The SEM images of AgNWs were then analyzed with OrientationJ, which is an ImageJ plug-in based on structure tensors.[43] The program computes the structure tensor for each pixel in the image and evaluates the local AgNW orientation. The cross-sectional images of the embedded AgNW lines in cured PDMS were obtained by the focused ion beam-scanning electron microscopy (FIB-SEM, Zeiss Auriga). The static contact angle measurements of the AgNW ink were performed using a goniometer (OCA 15, DataPhysics) at room temperature.

**2.7. Characterization of Electrical Performance.** Before examining the electrical performance of the fabricated conductors, the samples were thermally treated at 150 °C for 2 h. Then, a PDMS layer with a thickness of 500 $\mu$m was deposited via spin-coating on top of the printed samples to facilitate sample handling. The samples were then peeled off the PET substrate and placed on a PDMS substrate with a thickness of 1 mm for bending and stretching/releasing tests. The samples were kept for 4 h to ensure the two PDMS layers bond to each other. The edges of the samples were


https://dx.doi.org/10.1021/acsaelm.0c00616
ACS Appl. Electron. Mater. 2020, 2, 3289−3298

sputtered with gold and smeared with silver paste to make the contact points for electrical measurements.

## 3. RESULTS AND DISCUSSION

**3.1. Direct Inkjet Printing and Embedding of AgNWs into an Elastomer Substrate.** Figure 1 illustrates the inkjet

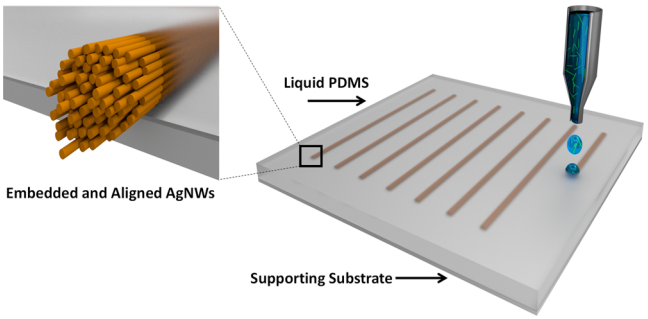


**Figure 1.** Illustration of the direct embedment of AgNWs into an uncured liquid elastomer layer by inkjet printing.

printing process to directly embed and align AgNWs in an uncured liquid PDMS layer. As shown in Figure 1, the AgNW ink was jetted onto the liquid PDMS layer, which was coated on a PET substrate in advance. Herein, the PET film was utilized as a supporting substrate for the liquid PDMS layer to facilitate the fabrication process of stretchable conductors as elaborated in detail in the following discussion. The ink–PDMS interactions, solvent evaporation, PDMS reflow, and assembly of AgNWs acted subsequently to eventually form an embedded line.

Such a fabrication process by inkjet printing and embedding requires a good understanding of the droplet impact and droplet–PDMS interactions. In this study, we first examined the impact and penetration behavior of the colloidal AgNW droplets into the liquid PDMS. For this task, a single AgNW colloidal droplet was jetted onto a thick liquid PDMS layer and photographed using a high-speed camera. As shown in Figure 2, upon the impact, the droplet spread at the surface of the liquid PDMS, producing a dent at the interface (i.e., surface deformation). The droplet then gradually penetrated the liquid PDMS interface to ~93 $\mu$m within ~138 ms and became completely embedded beneath the air–PDMS interface at ~453 ms. Afterward, the AgNW droplet lingered near the air–PDMS interface for a few seconds before it significantly shrank in its volume and continuously sank deeper into the liquid PDMS. It is interesting to note that droplet impact momentum does not contribute to the droplet penetration but the ethanol–PDMS interaction likely leads to the complete embedment of the colloidal droplet. This is confirmed by the finite element simulation of the droplet impact in COMSOL Multiphysics, where only 23 $\mu$m penetration depth was obtained because of the high viscosity of liquid PDMS (Figure S2 in the Supporting Information). On the other hand, the ethanol droplet became completely embedded in the liquid PDMS when gently deposited by a pipette with zero initial velocity (Figure S3), which directly supports that the embedment of the AgNW colloidal droplets is because of the ethanol–PDMS interaction. Surprisingly, the pure ethanol droplet did not experience the sinking behavior as compared to the AgNW colloidal droplet; instead, the droplet remained underneath the air–PDMS interface till the final stages of the solvent evaporation (Figure S4). The sinking of the AgNW droplets could be attributed to the ethanol evaporation and the AgNWs sinking into the liquid PDMS by the act of gravity.

Therefore, based on the results mentioned above, the embedment and assembly of the AgNWs in this study can be described by three steps: (i) droplet impact, where the jetted droplet undergoes droplet–PDMS interactions that prompts the droplet to settle beneath the air–PDMS interface; (ii) solvent evaporation and PDMS reflow, which assist in directing the assembly of AgNWs; and (iii) sinking and deposition of the AgNWs, where the ink–substrate interactions facilitates anchoring the AgNWs in the vicinity of the supporting substrate.

To understand the formation mechanism of the embedded AgNW lines, we investigated the effects of liquid PDMS layer thickness and the number of printing passes on the morphology and deposition depth of the printed AgNW lines in the liquid PDMS layer. Four different PDMS layer thicknesses were tested such as 1.5 mm, 250 $\mu$m, 100 $\mu$m, and 40 $\mu$m. For each film thickness, one to nine printing passes were examined. Figure 3 shows the printed AgNW lines for each layer thickness and various printing passes. Figure 4

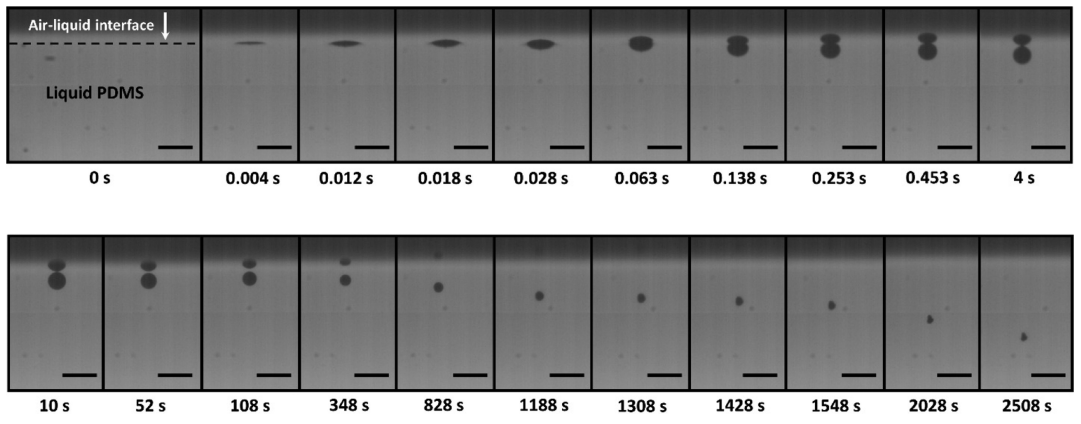


**Figure 2.** Image sequence demonstrating a single AgNW colloidal droplet impacting onto a thick PDMS layer. The droplet became fully embedded into the liquid PDMS after ~453 ms. The droplet remained stationary in vicinity of the air–PDMS interface for approximately 10 s prior to the sinking process. The secondary droplets shown above the droplets, particularly from 0.138 to 828 s, indicate the mirror reflection of the embedded droplets with the air–PDMS interface. The scale bar is 200 $\mu$m.



https://dx.doi.org/10.1021/acsaelm.0c00616
ACS Appl. Electron. Mater. 2020, 2, 3289–3298

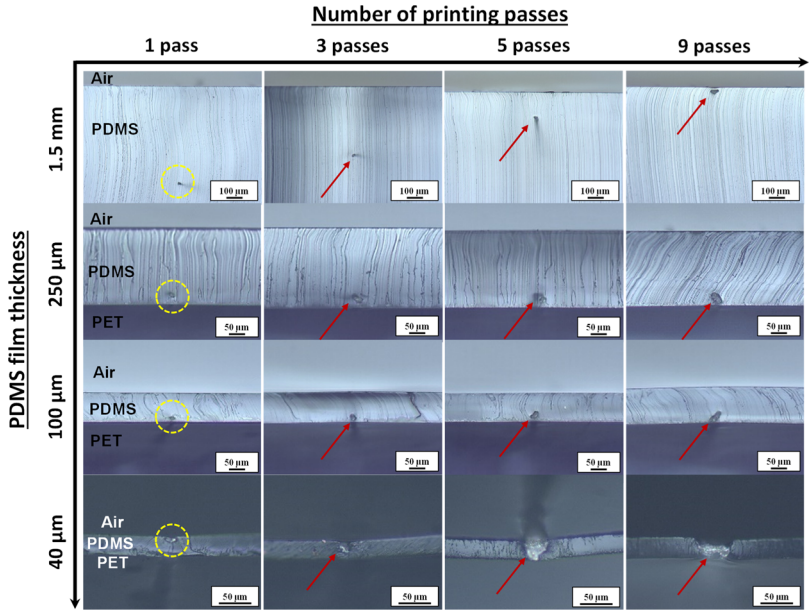


**Figure 3.** Optical images of the printed AgNW lines with respect to the number of printing passes and PDMS layer thickness. Different deposition depths of AgNW lines were obtained for various printing passes when utilizing a thick PDMS layer (i.e., 1.5 mm). However, the AgNW lines were found to deposit in the vicinity of the supporting PET substrate when using PDMS layer thickness equal or less than 250 $\mu$m. The yellow circles highlight the locations of the printed AgNW lines. The red arrows point to the printed AgNW lines for 3−9 passes.

illustrates different scenarios taking place for each layer thickness.

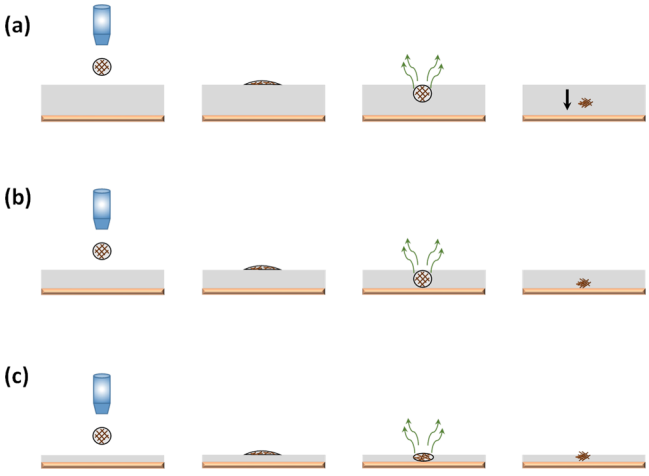


**Figure 4.** Illustration of the fabrication process of embedded AgNW lines. (a) Represents printing on a liquid PDMS layer with 1.5 mm thickness, which exemplifies the solvent evaporation and AgNW sinking processes. (b) Represents printing on a liquid PDMS layer with 100 $\mu$m thickness. (c) Represents the case of printing on a liquid PDMS layer with 40 $\mu$m thickness.

When the liquid film thickness of the elastomer was 1.5 mm, the AgNW lines were observed to form at different depths depending on the number of printing passes (the top row in Figure 3). In this system, once the jetted colloidal droplet of AgNWs and ethanol is encapsulated by the liquid PDMS, ethanol becomes surrounded by the liquid PDMS and can only escape the PDMS layer through the interface by evaporation. For this particular PDMS layer thickness (i.e., 1.5 mm), the AgNW line formation could be described by three stages. The primary stage consists of droplets' coalescence and interface penetration as a result of the droplet−PDMS interaction. The second stage is ethanol evaporation during which the AgNWs are retained in the vicinity of the surface of the PDMS layer, as shown in Figure 2 and illustrated in Figure 4. Increasing the number of printing passes means more solvent present underneath the air−PDMS interface, which maintains the AgNWs in the vicinity of PDMS surface during the solvent evaporation. The third stage is the AgNW line sinking process, which considerably depends on the number of printing passes. Thinner lines tend to sink more, while thicker lines tend to remain in the vicinity of the air−PDMS interface. This behavior could be attributed to the amount of ethanol embedded beneath the air−PDMS interface and the width of the printed line. Figure S5 demonstrates how printing with nine passes maintained the line near the air−PDMS interface during the solvent evaporation and AgNW assembly processes.

Decreasing the liquid PDMS layer thickness (e.g., 250 and 100 $\mu$m), however, produced different outcomes, where the printed AgNW lines deposited at the bottom of the liquid PDMS layer regardless the number of printing passes (Figures 3 and 4). When printing a single pass, the printed AgNWs sank and deposited onto the supporting PET substrate; while in printing multiple passes, the coalesced droplets were able to reach the supporting substrate. In this case, the ink−substrate interaction assisted in anchoring the colloidal droplets in place. Please note that the penetration depth of the printed AgNW line with nine passes has reached ~360 $\mu$m as shown in Figure S5. In other words, the ethanol could not retain the AgNWs to the air−PDMS interface during the evaporation process as a result of the ink−substrate interaction. This ink−substrate interaction will be further elaborated in the following section.

As the PDMS layer thickness decreased to 40 $\mu$m, the printed AgNW lines were not completely embedded beneath the PDMS surface (Figures 3 and 4). In this study, the inflight diameter of the jetted droplets was ~100 $\mu$m. Therefore, once colloidal droplets break through the thin PDMS layer and deposit on the surface of the supporting PET substrate, part of


https://dx.doi.org/10.1021/acsaelm.0c00616
ACS Appl. Electron. Mater. 2020, 2, 3289−3298

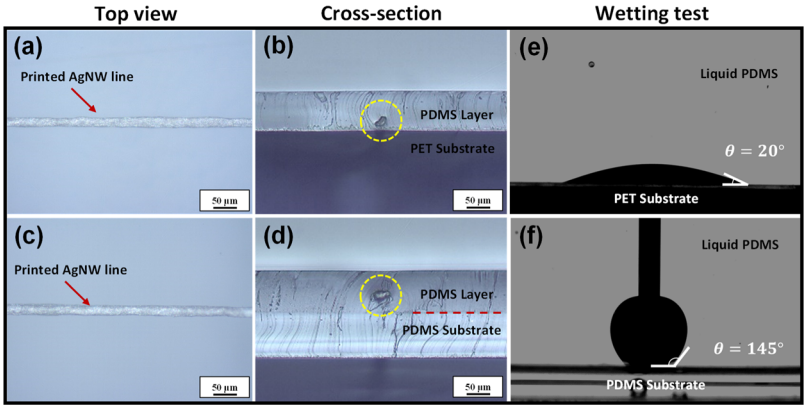


**Figure 5.** (a,b) Show the top and cross-sectional views of AgNW lines, printed with five passes into a PDMS layer with 100 $\mu$m thickness on a PET substrate. The printed line was deposited in the vicinity of the PET substrate. (c,d) Are the top and cross-sectional views of AgNW lines printed with five passes into a PDMS layer with 100 $\mu$m thickness, spin-coated on a cured PDMS substrate. (e,f) Present the contact angles of AgNW ink on the PET and PDMS substrates when submerged into liquid PDMS, indicating the stronger ink−substrate interactions on the PET substrate. Submerging the AgNW ink in liquid PDMS simulates the printed droplet in the liquid PDMS layers.

the droplet's cap remains above the PDMS layer, being exposed to air. In this case, the ethanol drags the rest of the droplets to the PDMS surface. As a result, the printed lines were located at top of the PDMS layer, producing a nonuniform, wavy morphology compared with those anchored at the supporting PET substrate (Figure S6). Thus, the thickness of the liquid PDMS layer is a critical parameter for the formation of embedded AgNW lines. PDMS films with thickness of ∼100 $\mu$m, which is comparable to the inflight diameter of the jetted droplet, produces the best results. During the inkjet printing process, the coalesced droplets reach the PET supporting substrate, where uniform AgNW lines can be generated and anchored at the bottom of the PDMS film (i.e., fully embedded) after solvent evaporation and PDMS curing. Furthermore, having a film thickness comparable to the droplet diameter facilitates the ethanol evaporation.

Figure S6 presents the morphology of the AgNW lines with respect to the number of printing passes. Occasionally, single pass produced broken lines because of possible missing jets. Three and five printing passes gave better results, and nine printing passes introduced too much ethanol, generating bulged and wavy lines. Therefore, in this study, five printing passes have been used to generate AgNW lines embedded into PDMS layers.

We have also examined the effect of the supporting substrate on the deposition depth of the printed AgNW lines. To compare with the PET substrate, a cured PDMS film was used as the supporting substrate. The embedded AgNWs were deposited in the middle of the elastomer layer after the printed samples were thermally cured. Figure 5a−d presents the top and cross-section views of the embedded AgNW lines under these two conditions. Figure 5e shows a contact angle of ∼20° of AgNW ink on the PET substrate, when immersed in the liquid PDMS to mimic the experimental conditions. This low contact angle indicates the strong adhesion of AgNW ink with the PET substrate. On the other hand, using a cured PDMS film as the supporting substrate gave different results. The AgNW ink exhibited a contact angle of ∼145° on the PDMS substrate, indicating its weaker adhesion (Figure 5f). In other words, the cured PDMS substrate resulted in poor ink−substrate interactions because of its low surface energy. Consequently, when the coalesced droplets reach and contact the supporting substrate, they would not stick to the cured PDMS substrate but migrate slightly upward during the solvent evaporation and curing processes. It should be noted that all the samples presented in Figures 3 and 5 were kept at room temperature for 30 min after printing, then thermally cured at 90 °C for 10 min.

Post-printing treatment, which affects the ethanol evaporation, is another crucial factor for controlling the location of the embedded AgNW lines. Three different post-printing treatment conditions were studied: (i) thermally curing the samples immediately after printing for 10 min at 90 °C, (ii) resting the samples for 30 min at room temperature then curing for 10 min at 90 °C, and (iii) curing the samples for 24 h at room temperature. It has been reported that liquid PDMS shows no curing ability in the presence of ethanol.[44] However, as the ethanol gradually evaporates, the PDMS layer can be fully cured by one of abovementioned processes.

It can be clearly seen from Figure 6a that printing followed by immediate thermal curing at 90 °C for 10 min pushed the AgNWs to the surface of the PDMS as ethanol was forced to quickly evaporate through the PDMS layer. Please note that the curing temperature in this study is beyond the boiling point of ethanol. The resultant lift force generated by the enforced ethanol evaporation, that is, the combined effect of the buoyant force and the quickly decreasing gravitational force, overcomes the ink−substrate interactions, pushing the printed lines to the top surface of the PDMS. However, for the latter two drying conditions (Figure 6b,c), the AgNWs sank and deposited onto the supporting substrate because the initial slow evaporation of ethanol could not push the AgNWs to the top surface of the elastomer. The viscosity of the freshly prepared PDMS increased from 3.11 to 3.54 Pa·s after a span of 30 min. After 30 min at room temperature, the ethanol evaporation probably has completed and the AgNWs have deposited in the vicinity of the supporting substrate. The heat treatment solidified the PDMS with the embedded AgNWs. Therefore, the printed AgNWs remained at the bottom of the PDMS layer, as shown in Figure 6b,c, and were fully embedded in the cured PDMS film.

It is worth pointing out that we have characterized the location of the embedded AgNWs and line shape using the optical microscopy. Although PDMS is translucent, the individual AgNWs could not be discerned in those optical images. Furthermore, because the AgNWs are completely


https://dx.doi.org/10.1021/acsaelm.0c00616
ACS Appl. Electron. Mater. 2020, 2, 3289−3298

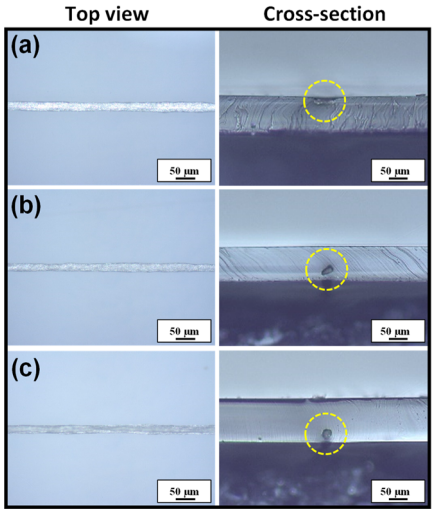


**Figure 6.** Optical images of the top and cross section of the AgNW lines with respect to curing conditions. (a) Shows the AgNW line lifted to the PDMS surface when the sample was immediately cured after printing. (b,c) Present embedded AgNW lines when the samples were retained for 30 min then cured at 90 °C for 10 min, and the samples cured at room temperature for 24 h, respectively. Five printing passes were used and the PDMS thickness is ∼100 $\mu$m.

embedded in the PDMS layer, it is challenging to examine the AgNWs under SEM because electrons could not penetrate the PDMS above the AgNWs lines (∼5−10 $\mu$m away from the side near the PET substrate). A SEM image of the cross section of a AgNW line prepared by razor blade cutting presents the challenge in the direct observation of the embedded AgNWs under the SEM, as shown in Figure S7. Therefore, FIB-SEM was utilized to examine the AgNW embedment in the cured PDMS.

**3.2. Alignment of the Embedded AgNWs.** In addition to the advantage of directly embedding AgNWs in an elastomer layer, this printing process aligns the AgNWs along the printing direction, which leads to desirable electrical performance for stretchable electronics. Figure 7a shows a schematic illustration of the formation mechanism of aligned AgNWs and a cross-sectional image of an embedded AgNW line after the FIB etching. The AgNWs were not tightly packed, however, the majority of them had circular cross sections indicating their orientation perpendicular to the etched interface (i.e., parallel to the line direction). Another FIB-SEM image is provided to show the complete embedment of the printed AgNW lines (Figure S8). Figure 7b−e shows the SEM images and the distribution of the AgNW orientation that demonstrate the alignment of AgNWs along the printing direction. In this case, the printed samples were soaked in cyclohexane to remove the uncross-linked PDMS in order to examine the microstructures of the AgNW assembly. The printed samples were retained at room temperature for 30 min before the cyclohexane soaking, which allowed the AgNWs to maintain the assembled line shape during soaking, supported by the fact that the linewidth of the embedded line in Figure 7a is similar to that in Figure 7b. The coalescence of the jetted droplets was controlled by utilizing 50 $\mu$m in-line spacing and a

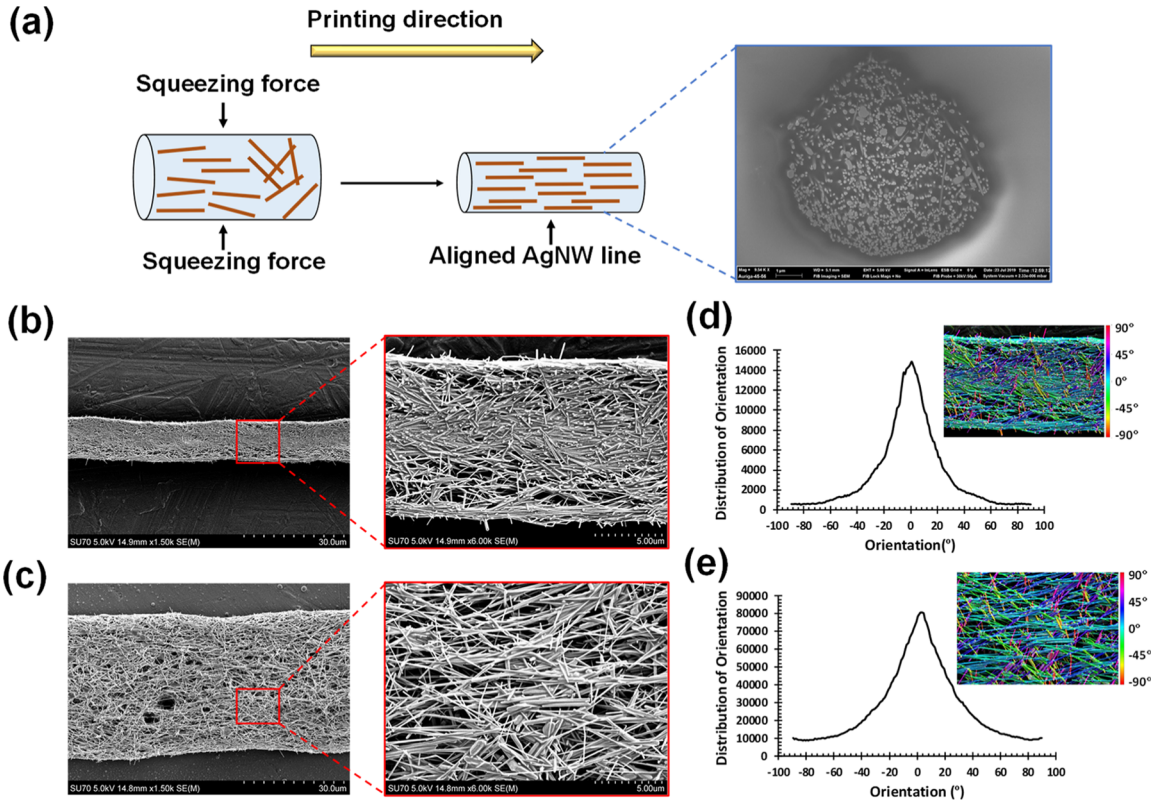


**Figure 7.** (a) Schematic illustration of the formation mechanism of aligned AgNWs and FIB-SEM cross-sectional image of an embedded AgNW line printed with a single pass. (b) SEM images of the AgNW lines printed with one pass. (c) SEM images of the AgNW lines printed with five passes. (d) Histogram of the AgNW orientation shown in (b). (e) Histogram of the AgNW orientation shown in (c). The insets in (d,e) are the HSB mapping images of the AgNWs.


https://dx.doi.org/10.1021/acsaelm.0c00616
ACS Appl. Electron. Mater. 2020, 2, 3289−3298

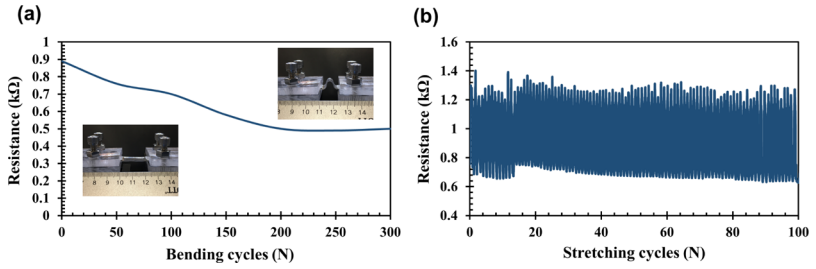


**Figure 8.** (a) Resistance change of embedded AgNW lines during the bending test. The line length is ∼25 mm and the bending radius is ∼6 mm. (b) Resistance change of embedded AgNW lines during 100 stretching/releasing cycles with a 10% strain. The samples were composed of two AgNW lines printed with five passes.

25 $\mu$m shift among the printing passes. During the printing process, the jetted droplets coalesce with an overlap of ∼50% to form connected lines because the inflight diameter of the colloidal droplet is ∼100 $\mu$m. As the ethanol solvent evaporates, the printed line shrinks, inside which the AgNWs are squeezed by the surrounding liquid PDMS. This squeezing force can align the AgNWs lengthwise parallel to the printing direction. Single printing pass gives a linewidth of ∼10 $\mu$m, where the alignment of AgNWs can be identified at both the center and the edge of the printed line (Figures 7 and S9). A color map of the processed SEM images (insets in Figure 7d,e) shows the hue, saturation, and brightness (HSB) representing the orientation, coherency, and the original source image, respectively. The histogram of the orientation quantitatively characterizes the degree of AgNW alignment. As shown in Figure 7d,e, the AgNWs are in general aligned along the printing direction. The line printed with a single pass has a narrower distribution with 78.9% of the AgNWs having an orientation angle of 30° or lower, compared with 65.8% for the line with 5 passes. We would like to point out that there is a shift of ∼3°, as shown in Figure 7e, because of the slight tilt of the original SEM image. To the best of our knowledge, this is one of the smallest AgNW linewidth obtained by printing methods as compared with the works reported elsewhere.[25,39,45−47] Three and five printing passes produced linewidths of ∼40 and 60 $\mu$m, respectively. This alignment of AgNWs along the printing direction may enhance the electrical performance during stretching/releasing cycles through increasing the wire-to-wire contact area.[48,49]

**3.3. Electrical Characterization of the Embedded AgNWs.** In order to evaluate the electrical performance of the embedded AgNW lines, bending and stretching/releasing tests were carried out on a homemade stretcher in the direction parallel to the longitudinal axis of the printed samples. Samples with two printed AgNW lines, made of five printing passes, were used for these tests. The bending radius used in this test was ∼6 mm, which makes a bending angle close to 150° (insets in Figure 8a). The initial resistance ($R_0$) of the fabricated sample is 0.88 kΩ with 25 mm line length. Figure 8a shows the change in resistance with respect to bending cycles. The resistance started to decrease after the first few bending cycles. After 50 bending cycles, the resistance dropped from 0.88 to 0.76 kΩ, which represents a 13.6% decrease of the initial resistance. This behavior could be attributed to the conditioning process of the AgNWs embedded in the elastomer, where they likely rearrange themselves to make more wire-to-wire contacts because of the cyclic deformation.[25,50,51] The printed AgNWs in this study are in general aligned along the printing direction (Figure 7d,e). However, they are not tightly packed (Figure 7a). The cyclic deformation in the elastomer may facilitate the formation of more contacts between the AgNWs. As a result, the resistance continued to decrease till reaching a plateau (∼43.2% of the initial resistance) at around 200 bending cycles. Beyond 300 cycles, the resistance measurements were not stable because the external silver paste contact joints degraded because of mechanical cracking. Nevertheless, the fabricated AgNW lines retained their integrity without any noticeable damage when examined under a light microscope. The fact that the embedded AgNW lines can survive hundreds of bending cycles indicates the effectiveness of elastomer encapsulation and the line robustness even with their small cross-sectional areas.

The same homemade stretcher was employed to test the electrical performance of the printed samples during multiple stretching/releasing cycles. The samples were strained up to 10% then released to the initial position for 200 cycles at a stretching rate of 0.2 mm $s^{-1}$, as shown in Figures 8b and S10. It should be mentioned that the initial resistance could vary slightly from one sample to another because of possible necking in the cross-sectional area of the printed wires. This behavior could be attributed to the possible missing jet droplets as a result of implementing only one printing station to fabricate the stretchable conductors. For the stretching/releasing test, the resistance ($R_0$) of the fabricated sample increased during the 10% strain to 1.30 kΩ then returned to the initial value (i.e., 0.76 kΩ), as demonstrated in Figure 8b. However, after the second stretching cycles, the resistance decreased from 0.76 to 0.68 kΩ, which corresponds to a 10.5% decrease of the initial resistance ($R_0$). After 90 stretching/releasing cycles, the resistance became stable, reaching a value of 0.63 kΩ, which represents a 17.1% decrease of the resistance. Similar to the bending test, this decrease in resistance is likely due to the local rearrangements of the AgNWs under the cyclic deformation. The conductors retained this stable resistance value till 180 stretching/releasing cycles, after which some high peaks were observed as a result of degradation of the external contact joints (Figure S10). The detailed resistance versus strain during the cyclic stretching is shown in Figure S11. The stable resistance of our fabricated stretchable conductors indicated the benefits of good alignment of AgNWs along the printing direction (i.e., the direction of the stretching/releasing test) and the PDMS encapsulation that significantly enhanced the AgNW recovery upon releasing the strain. As a proof-of-concept demonstration, these conductors have survived hundreds of bending and stretching cycles with the contact joints that were not optimized for microconductors. These results show the promise of this inkjet


https://dx.doi.org/10.1021/acsaelm.0c00616
ACS Appl. Electron. Mater. 2020, 2, 3289−3298

embedment approach for fabricating stretchable electronic conductors and sensors. For real applications, the embedded conductors can be fabricated directly onto pre-patterned electrodes.

**3.4. Discussion.** Direct inkjet embedding of AgNWs into an elastomer provides a facile approach to fabricate on-demand stretchable conductors. Different from printing of conductive inks on solid substrates, where the resolution of printed features is affected by substrate wettability and surface tension of the ink, in this study the shaping effect by the surrounding PDMS improves the printing resolution through generating lines with circular cross sections. As a result, it can produce conductors with tens of micrometers in linewidth or even smaller depending on the size of the printing nozzle. Compared with the conventional pattern-and-transfer methods, this approach eliminates the transferring step by directly patterning the conductive materials inside a stretchable elastomer, which significantly reduces the fabrication cost especially in manufacturing settings. Another advantage is the enhanced adhesion between the conductive materials and the elastomer layer. The embedded conductors overcome the issue with poor mechanical robustness of the AgNW/elastomer interface, where they buckled up after cyclic stretching/releasing.[25,52] The wrinkles and cracks developed at the surface of the elastomers and the AgNW/elastomer composites drastically affect the resistance of the printed patterns. By embedding the AgNWs directly inside the elastomer, the mechanical robustness and integrity of the printed patterns have been significantly enhanced. In lieu of silver nanoparticles in elastomers,[30] this work employed AgNWs, which enables desirable stretchability of the printed conductors. The AgNWs align along the printing direction by virtue of the isotropically compression, exerted by the surrounding liquid PDMS on the AgNW assembly as the solvent evaporates. In addition, tuning the elastomer layer thickness facilitates line formation through anchoring the printed patterns in the vicinity of the supporting substrate during solvent evaporation. This direct embedding process provides a novel printing platform for integrating different materials (e.g., hard or soft materials, magnetic, electrical, and mechanical materials, etc.) into soft host materials for heterogeneous structures and devices. It can also be incorporated into three-dimensional (3D) multi-materials printers as an add-on module for printing functional 3D architectures.

## 4. CONCLUSIONS

In summary, we have demonstrated the mechanisms and process controls to fabricate stretchable conductors by inkjet printing of AgNWs into an uncured liquid elastomer substrate in a single step. Colloidal ink of AgNWs dispersed in ethanol was directly printed into a liquid PDMS layer, supported by a PET substrate. The printing process was captured by high-speed photography to reveal the ink embedment and assembly process. The morphology and embedment depth of the AgNW lines are dictated by the thickness of the liquid PDMS layer.

Uniform lines were obtained for PDMS thickness close to 100 $\mu$m, where the AgNWs were anchored and assembled in the vicinity of the supporting substrate because of the ink–substrate interaction. For thick PDMS layers, the jetted droplets did not reach the bottom of the PDMS layer and the deposition depth of the printed lines varied depending on the amount of the ink material present inside the liquid PDMS. In this particular case, the assembly process of the AgNW lines undergoes three stages, which are line formation and embedment beneath the air–PDMS interface, solvent evaporation and PDMS reflow, and AgNW sinking and depositing onto the supporting substrate, respectively. The AgNW sinking determines the final deposition depth, and more printing passes lead to less sinking. The AgNWs printed with nine passes experience no sinking and deposit near the PDMS surface. For the PDMS film thickness much less than 100 $\mu$m, the printed AgNW lines are partially exposed to air without full embedment, and finally the AgNWs deposit on the PDMS surface.

When the jetted droplets coalesce and form lines with the assistance of the supporting substrate, the shaping effect of the surrounding PDMS generates fully embedded lines with aligned AgNWs, which not only enhances the mechanical robustness and integrity of the printed AgNW conductors but also improves their electrical performance during various bending and stretching/releasing cycles. This makes the direct embedment of AgNWs in elastomers by inkjet printing a promising venue for engineering flexible and stretchable conductors. It also represents a novel printing platform to integrate functional materials into soft materials for heterogeneous structures and devices.

## ■ ASSOCIATED CONTENT

### Supporting Information

The Supporting Information is available free of charge at https://pubs.acs.org/doi/10.1021/acsaelm.0c00616.

Morphology of the as-synthesized AgNWs; finite element simulation of droplet impact; embedment of an ethanol droplet dispensed with a pipette; image sequence of jetting an ethanol droplet onto a thick liquid PDMS layer; image sequence of printing AgNW lines with nine passes; optical images of the printed AgNW lines with various printing passes; SEM image of the cross-section of the embedded AgNW lines; FIB-SEM image of the cross-section of the embedded AgNW lines; SEM images of the AgNW lines after cyclohexane soaking; resistance change of the embedded AgNW lines for extended stretching/releasing cycles; and discussion on the conductivity and stretchability of the printed AgNW lines (PDF)

## ■ AUTHOR INFORMATION


### Corresponding Author

**Hong Zhao** − *Department of Mechanical and Nuclear Engineering, Virginia Commonwealth University, BioTech One, Richmond, Virginia 23219, United States;* orcid.org/0000-0001-9148-0158; Phone: 804-827-7025; Email: hzhao2@vcu.edu; Fax: 804-827-7030

### Authors

**Karam Nashwan Al-Milaji** − *Department of Mechanical and Nuclear Engineering, Virginia Commonwealth University, BioTech One, Richmond, Virginia 23219, United States*

**Qijin Huang** − *Department of Mechanical and Nuclear Engineering, Virginia Commonwealth University, BioTech One, Richmond, Virginia 23219, United States;* orcid.org/0000-0002-7390-6976

**Zhen Li** − *Department of Mechanical and Nuclear Engineering, Virginia Commonwealth University, BioTech One, Richmond, Virginia 23219, United States*




https://dx.doi.org/10.1021/acsaelm.0c00616
ACS Appl. Electron. Mater. 2020, 2, 3289−3298

**Tse Nga Ng** − *Department of Electrical and Computer Engineering, University of California, San Diego, La Jolla, California 92093, United States;* orcid.org/0000-0001-6967-559X

Complete contact information is available at: https://pubs.acs.org/10.1021/acsaelm.0c00616

### Author Contributions

[§]K.N.A.-M. and Q.H. contributed equally to this work.

### Notes

The authors declare no competing financial interest.

## ■ ACKNOWLEDGMENTS

This work is supported by Thomas F. and Kate Miller Jeffress Memorial Trust through Jeffress Trust Awards Program in Interdisciplinary Research.

## ■ REFERENCES

(1) Trung, T. Q.; Lee, N.-E. Recent Progress on Stretchable Electronic Devices with Intrinsically Stretchable Components. *Adv. Mater.* **2017**, *29*, 1603167.
(2) Huang, S.; Liu, Y.; Zhao, Y.; Ren, Z.; Guo, C. F. Flexible Electronics: Stretchable Electrodes and Their Future. *Adv. Funct. Mater.* **2019**, *29*, 1805924.
(3) Choi, S.; Han, S. I.; Kim, D.; Hyeon, T.; Kim, D.-H. High-Performance Stretchable Conductive Nanocomposites: Materials, Processes, and Device Applications. *Chem. Soc. Rev.* **2019**, *48*, 1566−1595.
(4) Yao, S.; Ren, P.; Song, R.; Liu, Y.; Huang, Q.; Dong, J.; O'Connor, B. T.; Zhu, Y. Nanomaterial-Enabled Flexible and Stretchable Sensing Systems: Processing, Integration, and Applications. *Adv. Mater.* **2020**, *32*, 1902343.
(5) Sim, K.; Rao, Z.; Ershad, F.; Yu, C. Rubbery Electronics Fully Made of Stretchable Elastomeric Electronic Materials. *Adv. Mater.* **2020**, *32*, 1902417.
(6) Liang, J.; Li, L.; Tong, K.; Ren, Z.; Hu, W.; Niu, X.; Chen, Y.; Pei, Q. Silver Nanowire Percolation Network Soldered with Graphene Oxide at Room Temperature and Its Application for Fully Stretchable Polymer Light-Emitting Diodes. *ACS Nano* **2014**, *8*, 1590−1600.
(7) Larson, C.; Peele, B.; Li, S.; Robinson, S.; Totaro, M.; Beccai, L.; Mazzolai, B.; Shepherd, R. Highly Stretchable Electroluminescent Skin for Optical Signaling and Tactile Sensing. *Science* **2016**, *351*, 1071−1074.
(8) Zhao, J.; Chi, Z.; Yang, Z.; Chen, X.; Arnold, M. S.; Zhang, Y.; Xu, J.; Chi, Z.; Aldred, M. P. Recent Developments of Truly Stretchable Thin Film Electronic and Optoelectronic Devices. *Nanoscale* **2018**, *10*, 5764−5792.
(9) Wang, S.; Xu, J.; Wang, W.; Wang, G.-J. N.; Rastak, R.; Molina-Lopez, F.; Chung, J. W.; Niu, S.; Feig, V. R.; Lopez, J.; Lei, T.; Kwon, S.-K.; Kim, Y.; Foudeh, A. M.; Ehrlich, A.; Gasperini, A.; Yun, Y.; Murmann, B.; Tok, J. B.-H.; Bao, Z. Skin Electronics from Scalable Fabrication of an Intrinsically Stretchable Transistor Array. *Nature* **2018**, *555*, 83−88.
(10) Park, D. H.; Park, H. W.; Chung, J. W.; Nam, K.; Choi, S.; Chung, Y. S.; Hwang, H.; Kim, B.; Kim, D. H. Highly Stretchable, High-Mobility, Free-Standing All-Organic Transistors Modulated by Solid-State Elastomer Electrolytes. *Adv. Funct. Mater.* **2019**, *29*, 1808909.
(11) Chen, D.; Lou, Z.; Jiang, K.; Shen, G. Device Configurations and Future Prospects of Flexible/Stretchable Lithium-Ion Batteries. *Adv. Funct. Mater.* **2018**, *28*, 1805596.
(12) Liu, W.; Song, M.-S.; Kong, B.; Cui, Y. Flexible and Stretchable Energy Storage: Recent Advances and Future Perspectives. *Adv. Mater.* **2017**, *29*, 1603436.
(13) Mackanic, D. G.; Chang, T.-H.; Huang, Z.; Cui, Y.; Bao, Z. Stretchable Electrochemical Energy Storage Devices. *Chem. Soc. Rev.* **2020**, *49*, 4466−4495.
(14) Wang, J.; Lin, M.-F.; Park, S.; Lee, P. S. Deformable Conductors for Human−Machine Interface. *Mater. Today* **2018**, *21*, 508−526.
(15) Trung, T. Q.; Lee, N.-E. Flexible and Stretchable Physical Sensor Integrated Platforms for Wearable Human-Activity Monitoring and Personal Healthcare. *Adv. Mater.* **2016**, *28*, 4338−4372.
(16) Wang, B.; Facchetti, A. Mechanically Flexible Conductors for Stretchable and Wearable E-Skin and E-Textile Devices. *Adv. Mater.* **2019**, *31*, 1901408.
(17) Xie, Z.; Avila, R.; Huang, Y.; Rogers, J. A. Flexible and Stretchable Antennas for Biointegrated Electronics. *Adv. Mater.* **2020**, *32*, 1902767.
(18) Wang, J.; Cai, G.; Li, S.; Gao, D.; Xiong, J.; Lee, P. S. Printable Superelastic Conductors with Extreme Stretchability and Robust Cycling Endurance Enabled by Liquid-Metal Particles. *Adv. Mater.* **2018**, *30*, 1706157.
(19) Han, F.; Su, X.; Huang, M.; Li, J.; Zhang, Y.; Zhao, S.; Liu, F.; Zhang, B.; Wang, Y.; Zhang, G.; Sun, R.; Wong, C.-P. Fabrication of a Flexible and Stretchable Three-Dimensional Conductor Based on Au-Ni@graphene Coated Polyurethane Sponge by Electroless Plating. *J. Mater. Chem. C* **2018**, *6*, 8135−8143.
(20) Peng, Y.; Xiao, S.; Yang, J.; Lin, J.; Yuan, W.; Gu, W.; Wu, X.; Cui, Z. The Elastic Microstructures of Inkjet Printed Polydimethylsiloxane as the Patterned Dielectric Layer for Pressure Sensors. *Appl. Phys. Lett.* **2017**, *110*, 261904.
(21) Lei, Z.; Wu, P. A. Highly Transparent and Ultra-Stretchable Conductor with Stable Conductivity during Large Deformation. *Nat. Commun.* **2019**, *10*, 3429.
(22) Huang, Q.; Zhu, Y. Printing Conductive Nanomaterials for Flexible and Stretchable Electronics: A Review of Materials, Processes, and Applications. *Adv. Mater. Technol.* **2019**, *4*, 1800546.
(23) Kim, D. C.; Shim, H. J.; Lee, W.; Koo, J. H.; Kim, D. H. Material-Based Approaches for the Fabrication of Stretchable Electronics. *Adv. Mater.* **2020**, *32*, 1902743.
(24) Jung, J.; Cho, H.; Yuksel, R.; Kim, D.; Lee, H.; Kwon, J.; Lee, P.; Yeo, J.; Hong, S.; Unalan, H. E.; Han, S.; Ko, S. H. Stretchable/Flexible Silver Nanowire Electrodes for Energy Device Applications. *Nanoscale* **2019**, *11*, 20356−20378.
(25) Huang, Q.; Al-Milaji, K. N.; Zhao, H. Inkjet Printing of Silver Nanowires for Stretchable Heaters. *ACS Appl. Nano Mater.* **2018**, *1*, 4528−4536.
(26) Xu, X.; Han, G.; Yu, H.; Jin, X.; Yang, J.; Lin, J.; Ma, C. Resistance Change of Stretchable Composites Based on Inkjet-Printed Silver Nanowires. *J. Phys. D: Appl. Phys.* **2020**, *53*, 05LT02.
(27) Xu, F.; Zhu, Y. Highly Conductive and Stretchable Silver Nanowire Conductors. *Adv. Mater.* **2012**, *24*, 5117−5122.
(28) Park, S.; Mondal, K.; Treadway, R. M., III; Kumar, V.; Ma, S.; Holbery, J. D.; Dickey, M. D. Silicones for Stretchable and Durable Soft Devices: Beyond Sylgard-184. *ACS Appl. Mater. Interfaces* **2018**, *10*, 11261−11268.
(29) Muth, J. T.; Vogt, D. M.; Truby, R. L.; Mengüç, Y.; Kolesky, D. B.; Wood, R. J.; Lewis, J. A. Embedded 3D Printing of Strain Sensors within Highly Stretchable Elastomers. *Adv. Mater.* **2014**, *26*, 6307−6312.
(30) Jiang, J.; Bao, B.; Li, M.; Sun, J.; Zhang, C.; Li, Y.; Li, F.; Yao, X.; Song, Y. Fabrication of Transparent Multilayer Circuits by Inkjet Printing. *Adv. Mater.* **2016**, *28*, 1420−1426.
(31) Hu, H.; Wang, S.; Wang, S.; Liu, G.; Cao, T.; Long, Y. Aligned Silver Nanowires Enabled Highly Stretchable and Transparent Electrodes with Unusual Conductive Property. *Adv. Funct. Mater.* **2019**, *29*, 1902922.
(32) Yang, B.-R.; Cao, W.; Liu, G.-S.; Chen, H.-J.; Noh, Y.-Y.; Minari, T.; Hsiao, H.-C.; Lee, C.-Y.; Shieh, H.-P. D.; Liu, C. Microchannel Wetting for Controllable Patterning and Alignment of Silver Nanowire with High Resolution. *ACS Appl. Mater. Interfaces* **2015**, *7*, 21433−21441.

(33) Takemoto, A.; Araki, T.; Noda, Y.; Uemura, T.; Yoshimoto, S.; Abbel, R.; Rentrop, C.; van den Brand, J.; Sekitani, T. Fine Printing Method of Silver Nanowire Electrodes with Alignment and Accumulation. *Nanotechnology* **2019**, *30*, 37LT03.
(34) Hu, H.; Pauly, M.; Felix, O.; Decher, G. Spray-Assisted Alignment of Layer-by-Layer Assembled Silver Nanowires: A General Approach for the Preparation of Highly Anisotropic Nano-Composite Films. *Nanoscale* **2017**, *9*, 1307−1314.
(35) Xu, Y.; Ge, D.; Calderon-Ortiz, G. A.; Exarhos, A. L.; Bretz, C.; Alsayed, A.; Kurz, D.; Kikkawa, J. M.; Dreyfus, R.; Yang, S.; Yodh, A. G. Highly Conductive and Transparent Coatings from Flow-Aligned Silver Nanowires with Large Electrical and Optical Anisotropy. *Nanoscale* **2020**, *12*, 6438−6448.
(36) Kang, S.; Kim, T.; Cho, S.; Lee, Y.; Choe, A.; Walker, B.; Ko, S.-J.; Kim, J. Y.; Ko, H. Capillary Printing of Highly Aligned Silver Nanowire Transparent Electrodes for High-Performance Optoelectronic Devices. *Nano Lett.* **2015**, *15*, 7933−7942.
(37) Li, X.; Kim, K.; Oh, H.; Moon, H. C.; Nam, S.; Kim, S. H. Cone-Jet Printing of Aligned Silver Nanowire/Poly(Ethylene Oxide) Composite Electrodes for Organic Thin-Film Transistors. *Org. Electron.* **2019**, *69*, 190−199.
(38) Lee, H.; Seong, B.; Kim, J.; Jang, Y.; Byun, D. Direct Alignment and Patterning of Silver Nanowires by Electrohydrodynamic Jet Printing. *Small* **2014**, *10*, 3918−3922.
(39) Finn, D. J.; Lotya, M.; Coleman, J. N. Inkjet Printing of Silver Nanowire Networks. *ACS Appl. Mater. Interfaces* **2015**, *7*, 9254−9261.
(40) Lu, H.; Lin, J.; Wu, N.; Nie, S.; Luo, Q.; Ma, C.-Q.; Cui, Z. Inkjet Printed Silver Nanowire Network as Top Electrode for Semi-Transparent Organic Photovoltaic Devices. *Appl. Phys. Lett.* **2015**, *106*, 093302.
(41) Huang, Q.; Shen, W.; Fang, X.; Chen, G.; Yang, Y.; Huang, J.; Tan, R.; Song, W. Highly Thermostable, Flexible, Transparent, and Conductive Films on Polyimide Substrate with an AZO/AgNW/AZO Structure. *ACS Appl. Mater. Interfaces* **2015**, *7*, 4299−4305.
(42) Coskun, S.; Aksoy, B.; Unalan, H. E. Polyol Synthesis of Silver Nanowires: An Extensive Parametric Study. *Cryst. Growth Des.* **2011**, *11*, 4963−4969.
(43) Rezakhaniha, R.; Agianniotis, A.; Schrauwen, J. T. C.; Griffa, A.; Sage, D.; Bouten, C. V. C.; van de Vosse, F. N.; Unser, M.; Stergiopulos, N. Experimental Investigation of Collagen Waviness and Orientation in the Arterial Adventitia Using Confocal Laser Scanning Microscopy. *Biomech. Model. Mechanobiol.* **2012**, *11*, 461−473.
(44) Miriyev, A.; Stack, K.; Lipson, H. Soft Material for Soft Actuators. *Nat. Commun.* **2017**, *8*, 596.
(45) Huang, Q.; Zhu, Y. Gravure Printing of Water-Based Silver Nanowire Ink on Plastic Substrate for Flexible Electronics. *Sci. Rep.* **2018**, *8*, 15167.
(46) Cui, Z.; Han, Y.; Huang, Q.; Dong, J.; Zhu, Y. Electrohydrodynamic Printing of Silver Nanowires for Flexible and Stretchable Electronics. *Nanoscale* **2018**, *10*, 6806−6811.
(47) Liang, J.; Tong, K.; Pei, Q. A Water-Based Silver-Nanowire Screen-Print Ink for the Fabrication of Stretchable Conductors and Wearable Thin-Film Transistors. *Adv. Mater.* **2016**, *28*, 5986−5996.
(48) Trotsenko, O.; Tokarev, A.; Gruzd, A.; Enright, T.; Minko, S. Magnetic Field Assisted Assembly of Highly Ordered Percolated Nanostructures and Their Application for Transparent Conductive Thin Films. *Nanoscale* **2015**, *7*, 7155−7161.
(49) Cho, S.; Kang, S.; Pandya, A.; Shanker, R.; Khan, Z.; Lee, Y.; Park, J.; Craig, S. L.; Ko, H. Large-Area Cross-Aligned Silver Nanowire Electrodes for Flexible, Transparent, and Force-Sensitive Mechanochromic Touch Screens. *ACS Nano* **2017**, *11*, 4346−4357.
(50) Kim, Y.; Zhu, J.; Yeom, B.; Di Prima, M.; Su, X.; Kim, J.-G.; Yoo, S. J.; Uher, C.; Kotov, N. A. Stretchable Nanoparticle Conductors with Self-Organized Conductive Pathways. *Nature* **2013**, *500*, 59−63.
(51) Cataldi, P.; Ceseracciu, L.; Marras, S.; Athanassiou, A.; Bayer, I. S. Electrical Conductivity Enhancement in Thermoplastic Polyurethane-Graphene Nanoplatelet Composites by Stretch-Release Cycles. *Appl. Phys. Lett.* **2017**, *110*, 121904.
(52) Chung, S.; Lee, J.; Song, H.; Kim, S.; Jeong, J.; Hong, Y. Inkjet-Printed Stretchable Silver Electrode on Wave Structured Elastomeric Substrate. *Appl. Phys. Lett.* **2011**, *98*, 153110.


https://dx.doi.org/10.1021/acsaelm.0c00616
*ACS Appl. Electron. Mater.* 2020, 2, 3289−3298